Solid Freeform Fabrication 2017: Proceedings of the 28th Annual International Solid Freeform Fabrication Symposium – An Additive Manufacturing Conference
Reviewed Paper

Effects of Area Fraction and Part Spacing on Degradation of 304L Stainless Steel Powder in Selective Laser Melting

Caitlin S. Kriewall[1], Austin T. Sutton[2], Sreekar Karnati[2], Joseph W. Newkirk[1], Ming C. Leu[2]

[1]Department of Materials Science and Engineering, Missouri University of Science and Technology, Rolla, MO 65409
[2]Department of Mechanical and Aerospace Engineering, Missouri University of Science and Technology, Rolla, MO 65409

Abstract

In selective laser melting (SLM) systems, a large portion of powder remains unconsolidated and therefore recycling powder could make SLM more economical. Currently, a lack of literature exists specifically targeted at studying the reusability of powder. Furthermore, the definition of powder reusability is complex since powder degradation depends on many factors. The goal of the current research is to investigate the effects of area fraction and part spacing on the degradation of 304L powder in SLM. An experimental study was conducted where various area fractions and part distances were chosen and powder characterization techniques for determination of particle size distributions, tap and apparent densities, and x-ray diffraction were employed to track evolving powder properties for the purpose of reuse. The results show that the recyclability of 304L powder depends on the utilization of the build area causing varying degrees of particle size coarsening and delta ferrite formation.

Introduction

Selective laser melting (SLM) is a powder bed fusion additive manufacturing (AM) technique where parts are built layer by layer. In this process, powder is dispensed and spread over a build plate at a predetermined thickness. A laser is then scanned over locations specified by a CAD model to consolidate the powder. After completion of the layer, the build plate is incremented down by one layer thickness and the process is repeated until the final part dimensions are achieved [1]. AM has attracted the interest of several industries due to its ability to make near net shaped parts with complicated geometry that are not attainable with subtractive processing technologies. However, powder bed processes inherently have a significant percentage of powder that is leftover after processing, as generally only 10%-50% of the build area is used for parts. Therefore, there is an opportunity to reuse this leftover powder, which would benefit the economy of the process as currently 5-46% of the cost of the SLM process is attributed to material costs [2]. However, powder characteristics and their effect on part properties must be well understood before widespread reuse of powder can be implemented.

Although sparse, there are some studies in the literature on the recyclability of certain metal powders including Ti64, Inconel 718, 17-4 PH stainless steel, and CoCr [3-5]. Tang *et al.* [3] studied the recyclability of Ti64 by creating a build of tensile specimens in an Arcam EBM system and collecting the powder after each build. The powder composition, size distribution, apparent and tap densities, flowability and morphology were examined after selected uses. They found that

the powder could be reused up to 21 times with no undesirable effects on the mechanical properties. Ardila *et al.* [4] studied the reusability of Inconel 718 on a Model Realizer SLM 250. Powder was collected after each iteration and the particle size distribution and composition was studied. Parts were also produced in order to evaluate the porosity, toughness, hardness and microstructure. It was found that the Inconel 718 powder could be reused up to 14 times with no significant effect on the part properties. Slotwinski *et al.* [5] studied the reusability of 17-4 PH stainless steel and CoCr powders in the SLM process. Although investigation of the mechanical properties was not discussed in this article, it was shown that reusing the powders corresponded with an increase of the particle size distribution. In all of these studies, the methodology behind the build design was not discussed; it was only presented as a certain build that was produced and iterated multiple times.

Heat-affected powders are created during the SLM process and can deposit in the build area [6]. The area of parts has an effect on the amount of heat-affected powders that are produced. As this powder has been shown to have a deleterious effect on part properties [6], the success of a recyclability study will depend on the amount of parts that are present in the build. The effect of the area fraction and part spacing of built parts on the powder properties was investigated in this study. This approach aims to be a simple way to design a recyclability study, as each of the builds is relatively small and would take a minimal amount of powder and machine time. This preliminary study can be used to assess the effect of different area fractions on powder degradation. Then, a build can be designed that takes into account the desired specimens and area fractions where powder changes are known to occur. In this way there is a better chance of actually capturing changes in part properties. This study could also aid in pinpointing the area fractions where there begins to be an effect on the part properties, if such a dependence is present in the material.

Experimental Methods

Gas-atomized 304L SS powder was purchased from LPW Technology with the chemical composition listed in Table 1. Prior to processing, the powder was passed through a 63 µm mesh sieve in order to breakup agglomerates and remove large particles that would have a negative effect on the layer thickness and uniformity. The powder was used to build parts on a Renishaw AM 250 SLM machine which contained a pulsed Nd-YAG laser with a Gaussian profile beam intensity and a wavelength of 1070 nm. The diameter of the beam spot on the powder bed was approximately 70 µm. The oxygen content in the build chamber was kept below 1000 ppm and the substrate temperature was held at 80°C. Finally, a constant volumetric argon gas flow of 400 ft^3/min was maintained across the build area during processing and was recirculated through the AM 250.

Table 1: Chemical Composition of 304L SS powder used as the starting material in this study

Element	C	Cr	Cu	Fe	Mn	N	Ni	O	P	S	Si
Wt%	0.018	18.4	< 0.1	Bal	1.4	0.06	9.8	0.02	0.012	0.005	0.6

Several builds were used in order to study the effect of area fraction and part spacing on the degradation of powder. Four of these builds consisted of 5x5 arrays of squares that were built at different area fractions, i.e. 12.5%, 25%, 50%, and 75% of the build chamber consisted of parts. This corresponded to squares with edge dimensions of 15 mm, 21 mm, 30 mm, and 36 mm for the 12.5%, 25%, 50%, and 75% builds. An important note is that the area fraction corresponds to the area enclosed by the 4 bolt holes as corners and not the entire base plate. An additional three builds were conducted in order to evaluate the part spacing on the degradation of the powder. These builds used a 50% area fraction with different arrays of squares built, i.e. 7x7, 9x9, and 11x11 with part spacings of 8 mm, 6 mm, and 5 mm respectively. These builds are illustrated in Figure 1. Each of the seven builds was replicated three times in order to study how the powder characteristics change with recycling. Powder was collected after each build from the overflow and build area, characterized, sieved, and then placed back into the AM 250 for the 2nd and 3rd iteration. No new powder was added for successive builds. For the first iteration of builds, the squares were built up to 5 mm tall meaning that the builds ranged in time from 4-24 hours. For each subsequent iteration, the height of the parts was decreased by 1.5 mm.

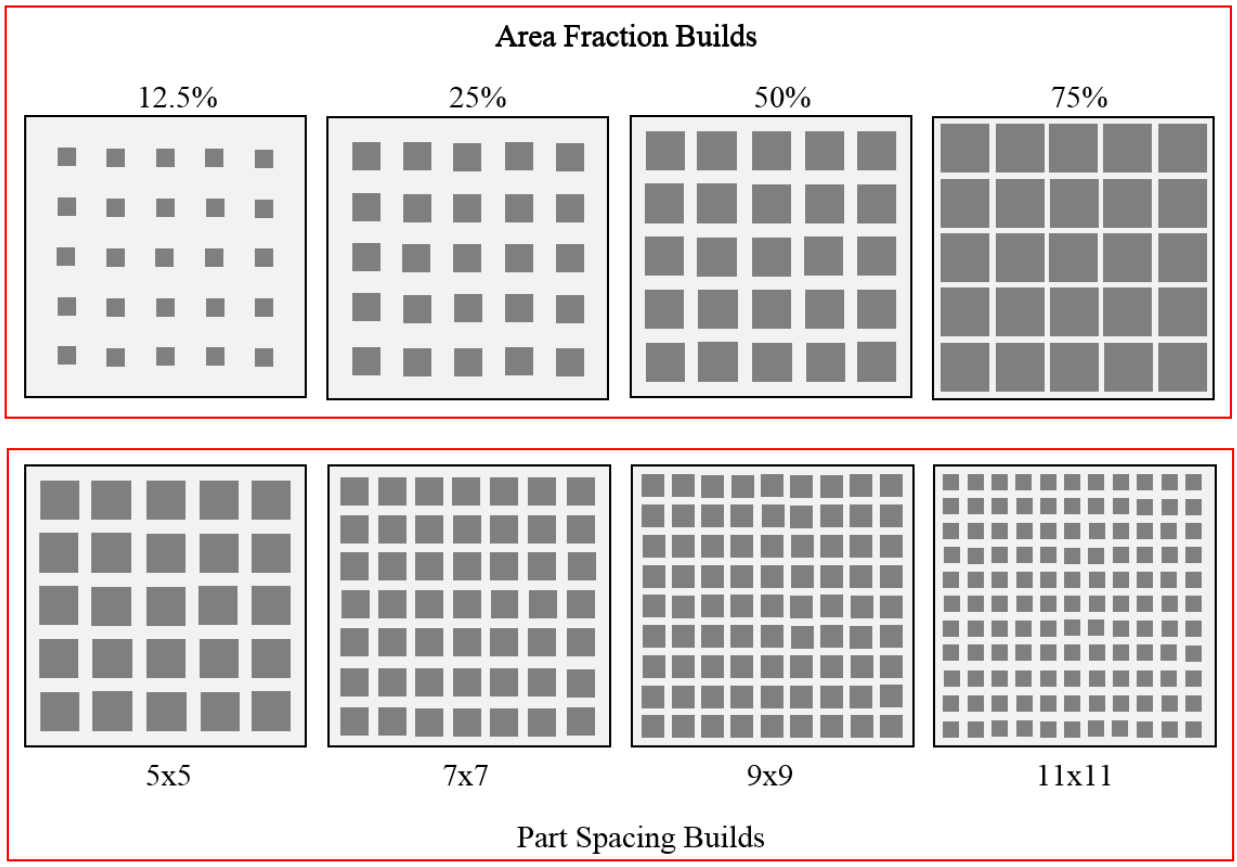

Figure 1: Illustration of the experimental builds. Note the 50% 5x5 build has been shown twice but was only completed once for each iteration. Part spacing builds were all at 50% area fraction.

As this work is designed to be a relatively quick and easy way to determine builds for a more vigorous powder recycling study, a limited selection of particle characterization techniques

were used and they were chosen based on the usefulness of the information and/or the ease of the measurement. The powder characterization included investigation of the particle size distributions, tap and apparent densities, and the phases present in the powder leftover from each build. Prior to any characterization, powder was mixed using a Turbula T2C mixer for a minimum of 15 minutes to ensure homogenization before sampling. Particle size distributions were obtained using an ASPEX 1020 scanning electron microscope (SEM) using the automated feature analysis (AFA) capabilities of the instrument. Each particle size distribution was generated from at least 2000 powder particles in order to establish an accurate distribution [7]. The particle size distributions were fit using JMP Pro software to obtain a 95% confidence interval of the distribution. Measurements of tap and apparent densities were conducted following ASTM standards B527-15 and B329-14 respectively. Each measurement of tap and apparent density was replicated three times. Determination of the percentage of phases was conducted using a Panalytical X'Pert Pro Multi-Purpose Diffractometer X-Ray Diffraction instrument. Due to the time and cost of the instrument, XRD scans were only obtained for samples of the 12.5%, 50% 5x5, 50% 11x11, and 75% builds in order to sample the extremes. XRD scans were performed from a 2θ range of 20-100 over a 3 hour period. RIQAS 4 software was used to perform the Rietveld refinement for quantification of phases. Finally, the powder after each build was sampled for testing and sieved through a 63 µm mesh sieve before the next build and the amount of powder sieved off was documented.

Results and Discussion

Particle size distributions have significant effects on the processing behavior of metal powders and have been shown to have an effect on the built part properties [8, 9]. The D10, D50, and D90 values from the numeric particle size distribution fit using JMP Pro are shown in Table 2. Here the plus or minus values show the 95% confidence interval. Each D-value corresponds to powder that is less than or equal to a certain size at the specified percentage. For example, the first iteration of the 12.5% area fraction build has a D50 value of 22.3 µm. This means that in the cumulative number plot, 50% of the powder was less than or equal to 22.3 µm. In order to make conclusions about the particle size distributions, the three D values must be considered together.

When considering the area fraction builds, both the D50 and D90 (shown in Figure 2 and Figure 3 respectively) values showed a statistically significant increase of the particle size between iteration 1 and 2. This increase was not observed for the D10 values, where for most cases (excluding the 50% 5x5), the D10 either was not statistically significantly different or there was a decrease observed. This coupled with the increase in D50 and D90 for the area fraction builds indicated that the particle size distributions were spreading out between iteration 1 and 2. However, this behavior was not carried into iteration 3, where the only area fraction build with a statistically significant increase in particle size distribution was the 25% build. The remaining area fraction builds showed a decrease in D90 values and either a decrease or no change in the D50 values. A trend was unable to be established for the D10 values between iteration 2 and 3. The coarsening observed between iteration 1 and 2 in the area fraction samples was not observed reliably in the part spacing samples. The 50% 5x5 build and the associated trends were discussed with regards to

the area fraction. Considering the 7x7, 9x9, and 11x11 builds, there was no trend found in the particle size distributions.

Table 2: D10, D50, and D90 values for each build and iteration.

Area Fraction	Array	D10 (µm)			D50 (µm)			D90 (µm)		
		Iteration 1	Iteration 2	Iteration 3	Iteration 1	Iteration 2	Iteration 3	Iteration 1	Iteration 2	Iteration 3
12.5%	5x5	13.8 ± 0.4	12.6 ± 0.7	15.4 ± 0.6	22.3 ± 0.3	24.9 ± 0.5	25.4 ± 0.4	30.8 ± 0.4	37.2 ± 0.7	35.4 ± 0.6
25%	5x5	11.6 ± 0.5	12.2 ± 0.4	13.6 ± 0.6	21.9 ± 0.4	23.8 ± 0.3	25.0 ± 0.5	32.3 ± 0.5	35.3 ± 0.4	36.4 ± 0.6
50%	5x5	14.7 ± 0.4	23.5 ± 0.3	14.5 ± 0.5	23.5 ± 0.3	28.6 ± 0.4	24.3 ± 0.4	32.4 ± 0.4	39.5 ± 0.5	34.2 ± 0.5
50%	7x7	17.5 ± 0.4	13.7 ± 0.5	14.5 ± 0.6	26.1 ± 0.3	25.2 ± 0.3	25.3 ± 0.4	34.7 ± 0.4	36.6 ± 0.5	36.1 ± 0.6
50%	9x9	14.3 ± 0.5	14.8 ± 0.4	11.2 ± 0.8	23.1 ± 0.4	24.9 ± 0.3	24.7 ± 0.6	31.8 ± 0.5	34.9 ± 0.4	38.2 ± 0.8
50%	11x11	15.1 ± 0.5	13.1 ± 0.7	14.5 ± 0.5	25.9 ± 0.4	24.8 ± 0.5	24.9 ± 0.4	36.6 ± 0.5	36.6 ± 0.7	35.4 ± 0.5
75%	5x5	14.3 ± 0.7	13.3 ± 0.9	15.1 ± 0.6	25.5 ± 0.5	28.3 ± 0.7	26.3 ± 0.5	36.6 ± 0.7	43.3 ± 0.9	37.5 ± 0.6

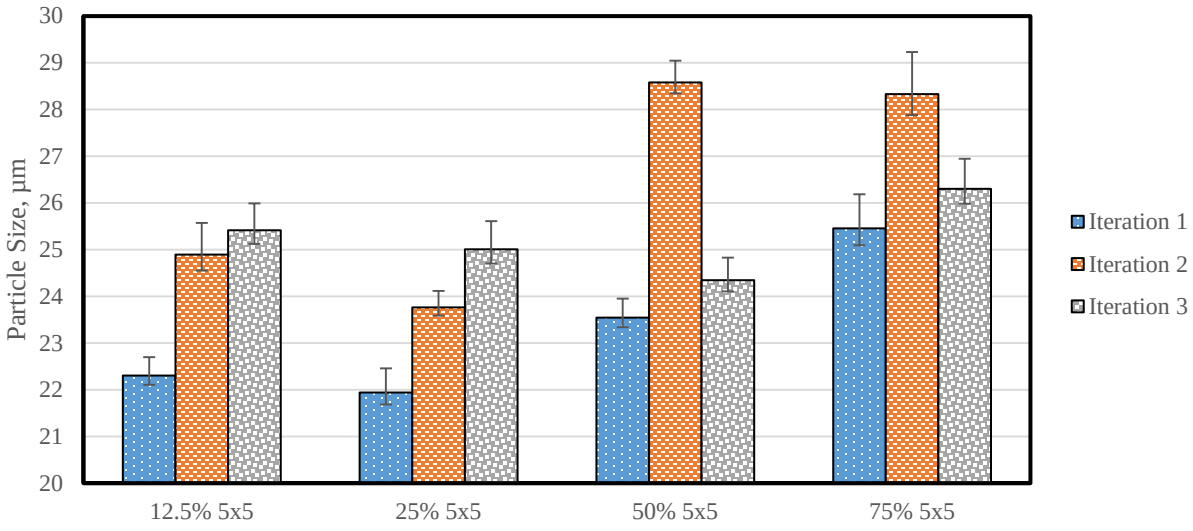

Figure 2: D50 values obtained from numeric particle size distributions for each iteration for the seven builds. Error bars show the 95% confidence intervals.

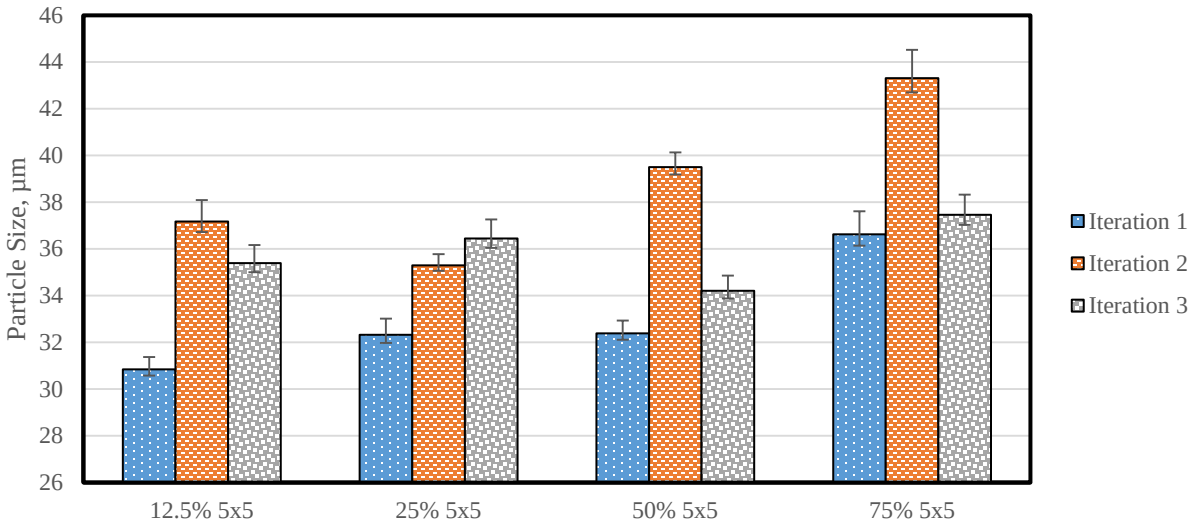

Figure 3: D90 values obtained from numeric particle size distributions for each iteration for the seven builds. Error bars show the 95% confidence intervals.

Table 3 shows the apparent density, tap density, and Hausner ratio of powder samples for each iteration, where the apparent and tap densities are graphically displayed in Figure 4 and Figure 5. Both the tap and apparent densities increased between iteration 1 and iteration 2 for all of the builds. Tap densities also increased between iteration 2 and iteration 3 in all cases except the 50% 9x9 build. However, the apparent densities dropped after iteration 2. With the increase of both the tap and apparent densities at iteration 2, a decrease in the Hausner ratio for certain builds (50% and 75%) was observed. The Hausner ratio is the ratio of the tap to apparent densities and serves as a simple way to describe the flowability of powders [10]. Although this ratio has been noted to be unsatisfactory in completely describing the flowability in AM processes, the decrease in Hausner ratio corresponds with improving powder flowability. Improvement of powder flowability with reuse has also been noted by other researchers using different materials [3]. This improved flowability could imply that the ideal powder may not be the virgin powder. As both the tap and apparent density values were increasing, the density of each powder layer and therefore the bed density was expected to improve as well [9]. This improved bed density could have a positive influence on the part density, as a more dense powder bed will increase the density of the part by decreasing the lack-of-fusion pores. Future work will incorporate part density measurements by Archimedes method in order to assess how the powder spreadability is changing with powder reuse.

Table 3: Apparent density, tap density, and Hausner ratio for each iteration of the seven builds.

Area Fraction	Array	Apparent Density			Tap Density			Hausner Ratio		
		Iteration 1	Iteration 2	Iteration 3	Iteration 1	Iteration 2	Iteration 3	Iteration 1	Iteration 2	Iteration 3
12.5%	5x5	4.17 ± 0.01	4.25 ± 0.01	4.13 ± 0.01	4.77 ± 0.01	4.92 ± 0.02	4.94 ± 0.01	1.16 ± 0.00	1.16 ± 0.01	1.20 ± 0.00
25%	5x5	3.96 ± 0.02	4.14 ± 0.01	4.10 ± 0.00	4.86 ± 0.01	4.95 ± 0.00	5.04 ± 0.01	1.20 ± 0.01	1.20 ± 0.00	1.23 ± 0.00
50%	5x5	4.10 ± 0.02	4.28 ± 0.01	4.28 ± 0.01	4.86 ± 0.03	5.00 ± 0.00	4.99 ± 0.02	1.19 ± 0.01	1.17 ± 0.00	1.17 ± 0.01
50%	7x7	4.05 ± 0.02	4.34 ± 0.01	4.19 ± 0.01	4.87 ± 0.02	4.95 ± 0.00	5.00 ± 0.00	1.20 ± 0.01	1.14 ± 0.00	1.19 ± 0.00
50%	9x9	4.12 ± 0.01	4.34 ± 0.01	4.18 ± 0.01	4.90 ± 0.04	5.03 ± 0.00	4.98 ± 0.01	1.18 ± 0.00	1.16 ± 0.00	1.19 ± 0.01
50%	11x11	4.15 ± 0.01	4.34 ± 0.00	4.25 ± 0.00	4.95 ± 0.00	4.98 ± 0.01	5.14 ± 0.01	1.18 ± 0.01	1.16 ± 0.00	1.21 ± 0.00
75%	5x5	4.12 ± 0.01	4.41 ± 0.00	4.25 ± 0.00	4.85 ± 0.00	5.05 ± 0.00	5.10 ± 0.00	1.20 ± 0.00	1.14 ± 0.00	1.20 ± 0.00

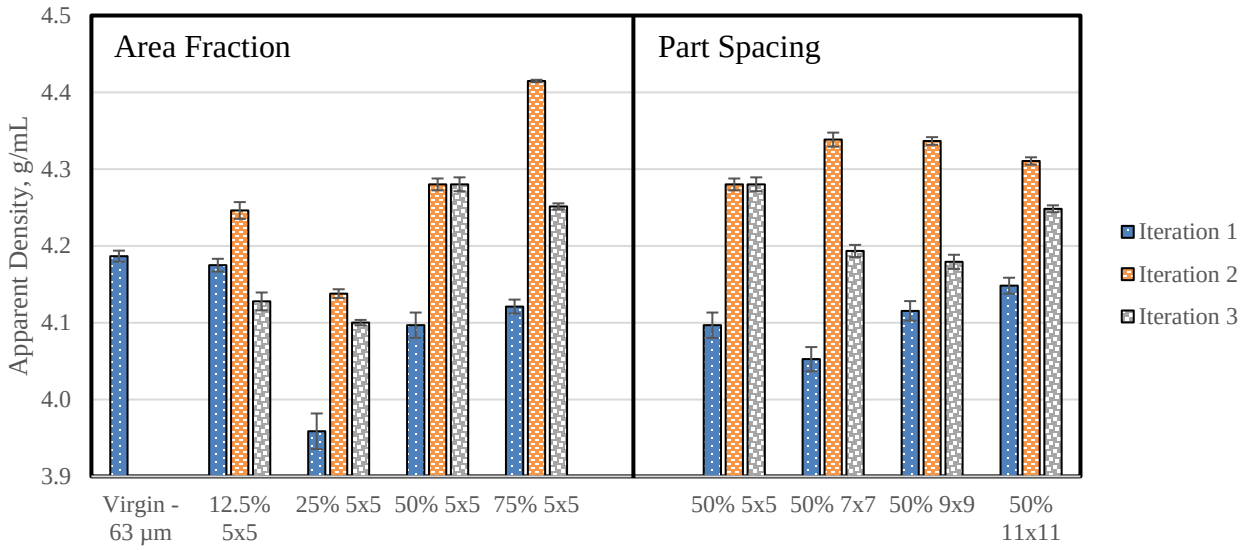

Figure 4: Apparent densities for various builds after each iteration. Error bars show the standard deviations of the three iterations.

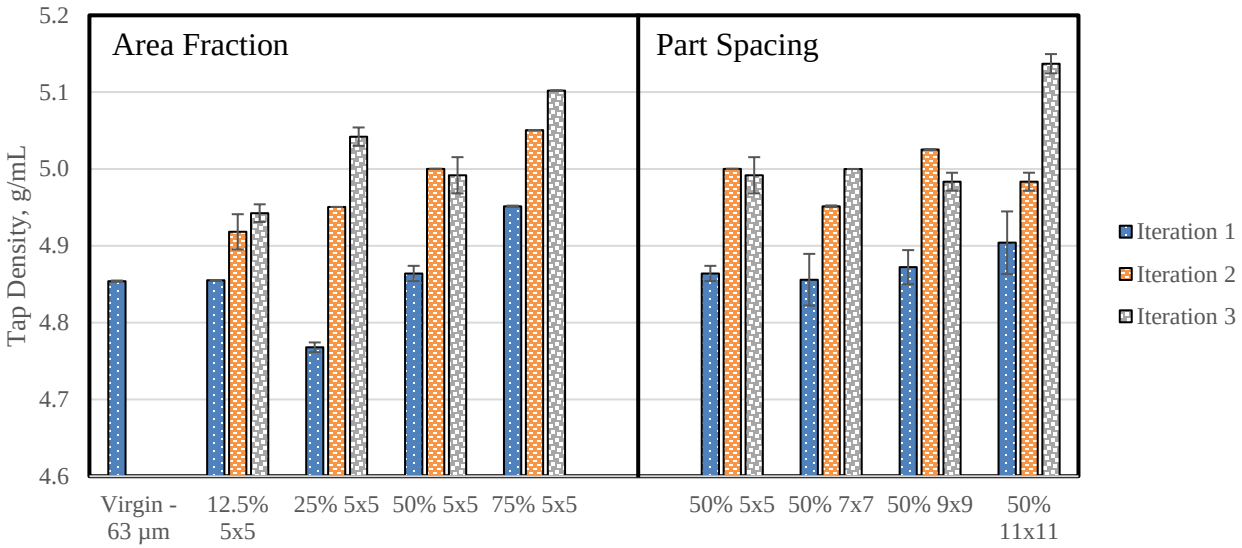

Figure 5: Tap densities for various builds after each iteration. Error bars show the standard deviations of the three iterations.

The results of the Rietveld refinement XRD pattern fitting on the 12.5%, 75%, 50% 5x5, and 50% 11x11 builds are shown in Table 4. In this table, the weight percentage of δ-ferrite is shown as each sample only had two identifiable phases, δ-ferrite and γ-austenite. 304L SS is an austenitic stainless steel that, according to the chrome nickel equivalent, follows a ferritic-austenitic solidification path where:

$$L \rightarrow L + \delta \rightarrow L + \gamma + \delta \rightarrow \gamma + \delta \rightarrow \gamma$$

where δ is δ-ferrite and γ is γ-austenite [11]. Fast cooling is necessary to retain δ-ferrite [12] however at extremely high cooling rates (on the order of $10^5 – 10^6$ K/s), the supercooled liquid can be present below the metastable solidus and solidification by primary austenite is possible [13]. Therefore, in the 304L SS powder processed through SLM, δ-ferrite becomes a marker of heat-affected powder, as the virgin powder has very little δ-ferrite due to the extremely high cooling rates achieved through the gas atomization process. In contrast, various kinds of heat-affected powder are present in the process due to the various interactions with the laser that have cooling rates sufficient to retain δ-ferrite [6]. For comparative purposes, the amount of δ-ferrite in the virgin 304L SS powder that had been passed through the 63 µm sieve was 1.5%.

When considering the area fraction builds (12.5% and 75%), there was an obvious difference in the amount of δ-ferrite present in the powder samples. In each iteration, the amount of δ-ferrite in the 75% build was always higher than in the 12.5% build. Both builds showed an increase, however the 75% build experienced a greater increase in δ-ferrite after each iteration. The part spacing builds are again more difficult to interpret, as there seems to be an anomalous result in the 50% 5x5 iteration 1. Comparisons between 50% 5x5 and the 11x11 builds do show that the 11x11 build has more δ-ferrite. Additionally, the amount of δ-ferrite increases with each iteration (for the 11x11 builds) and appears to increase at a faster rate than the 5x5 builds. These

results showed that both the area fraction and the part spacing have an effect on the amount of heat-affected powder that is generated and deposited inside the build chamber during processing.

Table 4: Rietveld refinement results for quantification of XRD spectra. Values shown are weight percent of δ-ferrite

Area Fraction	Array Size	Iteration 1	Iteration 2	Iteration 3
12.5%	5x5	0%	0.1%	1.3%
50%	5x5	2.2%	0.9%	1.1%
50%	11x11	4.2%	4.9%	6.1%
75%	5x5	3.6%	7.2%	11.4%

Figure 6 shows the results of the percentage of powder that was sieved off prior to being run for the next iteration. Between iteration 1 and 2, more powder was generally sieved off, although the amount sieved off for the 12.5% build stayed consistent. Furthermore, between iteration 2 and 3 the majority of the samples either stayed the same or decreased in the amount of powder sieved off, although the 50% 5x5 and 9x9 builds still increased. This result was consistent with what was observed from the particle size distributions. When considering the different area fractions, there was a clear trend that increasing the area fraction corresponds to an increase in the amount of powder that was sieved out. Again, it was more difficult to establish a trend concerning the part spacing builds.

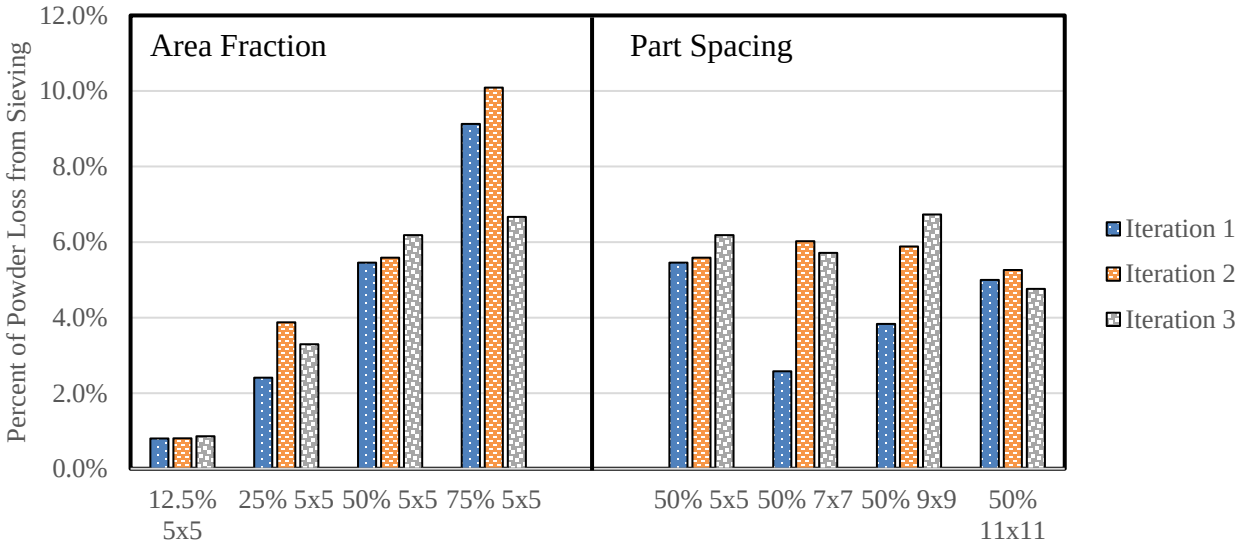

Figure 6: Percentage of powder sieved off after each iteration of builds.

Powder from any of these builds has been shown to change in at least one of the characterizations performed. However, the degree to which it changes was different for each build. For the 12.5% area fraction builds, the change was noted in the particle size distributions and tap and apparent densities, yet the XRD and percent of powder sieved off show fairly consistent

powder with minor differences (where the amount sieved off increased from 0.8% to 0.9% and the weight percent of δ-ferrite increased by only 1.3%). On the other hand, the 75% powder showed differences in every test, however a 75% area fraction build would be difficult to justify for a recycling study as the first build would have to be repeated several times in order to generate enough powder to carry through the study, depending on how many iterations would be needed. A 304L SS powder reusability study incorporating more mechanical testing and powder characterization parts will be employed. Area fractions between 25% and 50% will be used for this study, because powder in this range has detectable differences that have been shown by other researchers to have an effect on the part properties.

Summary and Remarks

Powder characterization of the area fraction builds (12.5%, 25%, 50%, and 75%) and part spacing builds (50% 5x5, 7x7, 9x9, and 11x11) that were replicated three times enabled insights into the effect of area fraction on the powder. These included that increasing the area fraction induced an increase in the D50 and D90 of the particle size distributions between iteration 1 and 2. The corresponding D10 values stayed consistent or lowered, meaning that the particle size distributions were not only coarsening, but also widening. However, this behavior was not carried into iteration 3, where particle size distributions were shown to drop, yet the D50 and D90 were still higher for iteration 3 compared to iteration 1. Tap and apparent densities both increased between iteration 1 and 2 for all of the area fraction builds. This improvement in tap and apparent densities coupled with the spreading of the powder could have an advantageous effect as the powder bed density was expected to increase. While the tap density increased further on iteration 3, the apparent density either remained consistent or fell to a lower value for this iteration. The XRD analysis showed that the 75% area fraction had more δ-ferrite, an indication of the amount of heat-affected powder, than both the 12.5% and 50% area fraction builds. Finally, the amount of powder sieved off increased with increasing area fraction for all iterations. When comparing the same build through different iterations, the amount of powder sieved off was shown to increase between iteration 1 and 2 apart from the 12.5% area fraction that stayed consistent. Furthermore, between iteration 2 and 3 the powder sieved off was not as consistent, where 12.5% build stayed consistent, 25% and 75% decreased, and 50% increased. The amount of powder sieved was shown to change significantly for the 75% build with each iteration however the 12.5% build stayed consistent through each iteration.

Across all the powder characterization techniques employed it was more difficult to establish trends with the part spacing builds. Trends were not identifiable in the particle size distribution data. The same trends observed in the area fraction builds concerning the tap and apparent densities were observed in the part spacing builds. The XRD showed that the 11x11 builds had more δ-ferrite compared to the 5x5 build and the amount of δ-ferrite in the 11x11 build increased with each iteration. Finally, the sieving results showed no trend when comparing the different part spacing builds, however, when comparing iteration 1 to 2 there was an increase in the powder sieved off for each part spacing build. The 5x5 and 9x9 showed an increase in the

amount of powder sieved off between iteration 2 and 3 while builds 7x7 and 11x11 had a decrease in the amount of powder sieved off.

Powder from each of the builds was shown to have differences in at least one of the characterizations performed, however the degree to which the powder changed was different. The 75% build showed the most drastic differences, however this area fraction would be unrealistic for a more involved reusability study. For the more involved 304L SS powder reusability study, area fractions between 25% and 50% will be used given that the powders in this range did show detectable differences that could have an effect on part properties. Future work will involve powder characterization on samples post-sieving to correlate the heat-affected powder to the sieve loss. Additionally, mechanical testing will be needed to evaluate whether the differences observed in the powder equate to differences in part performance. For this testing, mini-tensile specimens will be extracted at 5 locations corresponding to the diagonal across the build plate. Comparisons between each build and iteration and the different builds will be completed. Ideally, this work will provide a way to optimize the powder loss to machine productivity trade-off. Finally, a more involved 304L SS powder reusability study will be performed.

Acknowledgments

This work was funded by Honeywell Federal Manufacturing & Technologies under Contract No. DE-NA0002839 with the U.S. Department of Energy. The United States Government retains and the publisher, by accepting the article for publication, acknowledges that the United States Government retains a nonexclusive, paid up, irrevocable, world-wide license to publish or reproduce the published form of this manuscript, or allow others to do so, for the United States Government purposes.

Furthermore, the authors would like to acknowledge Jeff Hill, Jacob Ficht, and Eric Bohannan for their assistance in this research.

References

[1] A. T. Sutton, C. S. Kriewall, M. C. Leu, and J. W. Newkirk, “Powder characterisation techniques and effects of powder characteristics on part properties in powder-bed fusion processes,” *Virtual Phys. Prototyp.*, vol. 12, no. 1, pp. 3–29, 2016.

[2] M. Barclift, S. Joshi, T. Simpson, and C. Dickman, “Cost modeling and depreciation for reused powder feedstock in powder bed fusion additive manufacturing,” *Solid Free. Fabr. Symp.*, pp. 2007–2028, 2016.

[3] H. P. Tang, M. Qian, N. Liu, X. Z. Zhang, G. Y. Yang, and J. Wang, “Effect of Powder Reuse Times on Additive Manufacturing of Ti-6Al-4V by Selective Electron Beam Melting,” *Jom*, vol. 67, no. 3, pp. 555–563, 2015.

[4] L. C. Ardila, F. Garciandia, J. B. González-Díaz, P. Álvarez, a. Echeverria, M. M. Petite, R. Deffley, and J. Ochoa, “Effect of IN718 Recycled Powder Reuse on Properties of Parts Manufactured by Means of Selective Laser Melting,” *Phys. Procedia*, vol. 56, pp. 99–107,

2014.

[5] J. A. Slotwinski, E. J. Garboczi, P. E. Stutzman, C. F. Ferraris, S. S. Watson, and M. A. Peltz, “Characterization of metal powders used for additive manufacturing,” *J. Res. Natl. Inst. Stand. Technol.*, vol. 119, pp. 460–493, 2014.

[6] A. Ladewig, G. Schlick, M. Fisser, V. Schulze, and U. Glatzel, “Influence of the shielding gas flow on the removal of process by-products in the selective laser melting process,” *Addit. Manuf.*, vol. 10, pp. 1–9, 2016.

[7] E. Vigneau, C. Loisel, M. F. Devaux, and P. Cantoni, “Number of particles for the determination of size distribution from microscopic images,” *Powder Technol.*, vol. 107, no. 3, pp. 243–250, 2000.

[8] P. K. Samal and J. W. Newkirk, “Powder Metallurgy, Metal Powder Characterization, Bulk Properties of Powders,” *ASM Handb.*, vol. 7, pp. 93–168, 2015.

[9] a B. Spierings, N. Herres, G. Levy, and C. Buchs, “Influence of the particle size distribution on surface quality and mechanical properties in AM steel parts,” *Rapid Prototyp. J.*, vol. 17, no. 3, pp. 195–202, 2011.

[10] H. H. Hausner, “Friction Conditions in a Mass of Metal Powder.pdf.” International Journal of Powder Metallurgy, pp. 7–13, 1967.

[11] A. F. Padilha, C. F. Tavares, and M. A. Martorano, “Delta Ferrite Formation in Austenitic Stainless Steel Castings,” *Mater. Sci. Forum*, vol. 730–732, pp. 733–738, 2012.

[12] K. Guan, Z. Wang, M. Gao, X. Li, and X. Zeng, “Effects of processing parameters on tensile properties of selective laser melted 304 stainless steel,” *Mater. Des.*, vol. 50, pp. 581–586, 2013.

[13] R. N. Wright, J. E. Flinn, G. E. Korth, J. C. Bae, and T. F. Kelly, “The microstructure and phase relationships in rapidly solidified type 304 stainless steel powders,” *Metall. Trans. A*, vol. 19, no. October, pp. 2399–2405, 1988.